Phys. Status Solidi B **249**, No. 4, 812–817 (2012) / **DOI** 10.1002/pssb.201147327

physica status solidi b
www.pss-b.com
basic solid state physics

Metal–semiconductor transition in $Sm_xMn_{1-x}S$ solid solutions

Sergey Aplesnin[1,2], Oxana Romanova[*,1,2], Anton Har'kov[1,2], Dmitrii Balaev[1], Michail Gorev[1], Alexander Vorotinov[1], Vladimir Sokolov[3], and Andrey Pichugin[3]

[1] Kirensky Institute of Physics, Russian Academy of Sciences, Siberian Branch, Akademgorodok 50, Bld. 38, Krasnoyarsk 660036, Russia
[2] Siberian State Aerospace University, Krasnoyarsk 660014, Russia
[3] Institute of Inorganic Chemistry, Russian Academy of Sciences, Siberian Branch, Novosibirsk 630090, Russia

Received 29 June 2011, revised 21 September 2011, accepted 3 November 2011
Published online 13 December 2011

Keywords Kondo effect, metal–semiconductor transition, semiconductors, variable-valence elements

* Corresponding author: e-mail rob@iph.krasn.ru, Phone: +(391)2907108, Fax: +(391) 2438923

The electrical resistivity of the $Sm_xMn_{1-x}S$ ($0.15 \le x \le 0.25$) solid solutions in the temperature range of 80–300 K was measured. Minimum and maximum in the temperature dependence of the resistivity were found, respectively, at $T = 220$ K for $x = 0.15$ and at $T = 100$ K for $x = 0.2$ compounds. This behavior is explained from the result of the mobility-edge movement, the disorder being due to elastic deformation and spin density fluctuations with short-range order. Metal–semiconductor phase transition versus concentration at $x_c = 0.25$ is observed. Resistivity is described by scattering electrons with acoustic phonon mode and with localized manganese spin. From the thermal expansion coefficient the compression of the lattice below the Néel temperature for $Sm_{0.2}Mn_{0.8}S$ is found.

1 Introduction In recent years particular attention has been focused on investigating the metal–semiconductor transition and magnetoelectric effect [1, 2]. Among the substances with the strong correlation between the magnetic and electrical properties are the disordered systems that reveal these effects. The creation of the novel materials having these properties makes it possible to solve problems of magnetic storage of information for microelectronics including spintronics [3].

Rare-earth chalcogenides crystallized in the NaCl-type structure and relate to semiconduction if the rare earth ion is in the divalent state and metallic when it is trivalent [4–6]. A semiconductor–metal phase transition is observed in samarium monosulfide under the action of pressure and when the decrease in the volume of SmS under the action of the applied field reaches a critical value of 4–5% at $T = 300$ K [7].

Samarium has an outer electronic configuration $4F^6 5S^2 5p^6 5d^0 6s^2$ and sulfur $3s^2 3p^4$. In rare-earth chalcogenides the d-levels are broadened into a band that hybridizes with the 6s band, while the localized 4f wave functions remain more or less the same as in the atom [8]. When hydrostatic pressure is applied to SmS the lower of crystal-field split a bands and its energy gap relative to the highest f level decreases until the f level and the d-band edge cross [9]. A semiconductor–metal transition takes place near the pressure where the f–d gap tends to zero. This transition involves delocalization of a 4f electron from the samarium ion ($4f^6 5d^0$–$4f^5 5d^1$) as the valence state change from 2+ to 3+. The ionic radius $Sm^{2+}(4f^6)$ is almost 20% larger than the ionic radius of $Sm^{3+}(4f^5)$.

The metallic state may also be induced by alloying with RE ions with radii of smaller size than Sm^{2+} [10]. The amount of crystal-field splitting is generally believed to increase when the lattice constant becomes smaller. The series of solid solutions, $Sm_{1-x}Y_xS$ and SmS, for example, have been widely studied [11]. In each of these systems, a discontinuous transition to a strongly homogeneous mixed-valent configuration occurs at an approximate compound of $x = 0.15$. On the other hand, the substitution of small, divalent Yb for Sm^{2+} does not lead to any valence mixing at all, and the substitution of relatively large trivalent ions (La^{3+} for Sm^{2+} or Sb^{3-} for S^{2-}) results in a weak, continuous transition to mixed valence. It is clear

that the electronic structures as well as the size of a replacing ion are important factors degree of valence mixing in SmS. MnS and SmS sulfides possess a crystal structure of NaCl-type fcc lattice with constant lattice $a = 5.222$ Å (MnS) [12] and $a = 5.965$ Å (SmS) [13] that is fall drop under pressure. One might expect that upon cation substitution of manganese ions by samarium ions the pressure imposed by the nearest neighborhood may induce electrons in the d-band that causes a number of phase transitions, both magnetic and electrical. Another important factor in the mixed-valent metallic state is the Kondo resonance observed in angle-resolved photoemission experiments [14] for a heavy-fermion system.

The Kondo resonance at the Fermi level of a heavy-fermion metal is due to hybridization of strongly correlated f orbitals with a metallic host, with characteristic high- and low-energy features in photoemission spectroscopy [15]. The increase of this hybridization then leads to a strongly mixed-valent state. Another group of compounds which gets to the same Anderson lattice class are the Kondo hybridization gap insulators. Experimentally, the Kondo insulating behavior is known to be very sensitive to the applied magnetic field [16], and the pressure [17]. It has been shown recently that the width of the "Kondo resonance" calculated based on the periodic Anderson model and the single-impurity Anderson model gives a measure of the "coherence temperature T_C" and the "Kondo temperature T_K", respectively. As a result, there are two energy scales in the problem with T_C suppressed compared to T_K, and this results in a pseudogap below the temperature T_C [18, 19].

The aim of this work is to study the possibility of the Kondo effect appearing and the semiconductor–metal transition in $Sm_xMn_{1-x}S$ solid solution consisting of ions with variable valence and to establish the mechanism of the electrical resistivity and interrelation between the electric, magnetic, and elastic subsystems.

2 Experimental results and discussion Phase composition and the crystal structure of the $Sm_xMn_{1-x}S$ samples were determined with a DRON-3 X-ray diffractometer in CuKα radiation at 300 K. The X-ray diffraction analysis shows that the synthesized $Sm_xMn_{1-x}S$ samples are single phase with a NaCl-type cubic lattice typical of α-MnS. X-ray data have already been presented [20]. The measured lattice parameters of $Sm_xMn_{1-x}S$ are shown in Fig. 1. With an increase in concentration x of the cation substitution, the a parameter of the unit cell grows from 0.5222 nm for α-MnS to 0.5307 nm for $Sm_{0.25}Mn_{10.75}S$ as the ionic radius of the substituent increases. The thick line connecting the pure compounds MnS and SmS under a pressure of 6.5 kbar represents Vegard's rule – those lattice parameters expected of a simple hard-sphere mixing of metallic SmS and MnS. All measured lattice parameters are seen to lie along the Vegard line, indicating that the samarium cations remain close to trivalence state. The resistivity of the MnS pure single crystals is independent of temperature at $T < T_N$ and behaves analogously to semiconductors up to 500 K with values of activation energy equal to $E_a = 0.2$ eV. The

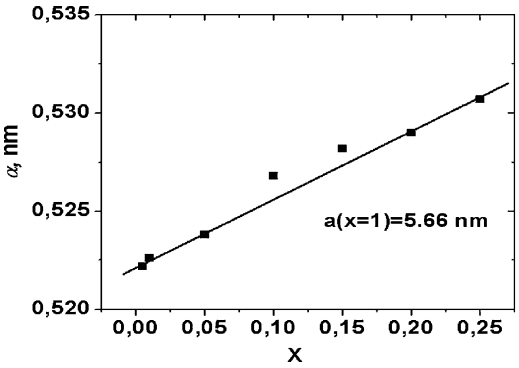

Figure 1 Concentration dependence of the lattice constant a for the $Sm_xMn_{1-x}S$ solid solution. Vegard's rule is denoted by the thick line.

temperature dependences (in the range 80–1000 K) of the electrical conductivity in SmS indicate that the absolute gap Δ between the 4f levels and the conduction-band edge of SmS is $\Delta = 0.23$–0.25 eV. The golden phase of SmS could be a narrowgap semiconductor. Evidence for a gap comes from the activation behavior of the electrical resistivity and point-contact measurements [21]. The estimations from the point-contact spectra show a possible gap of about 6.4 meV [21]. On the other hand, some experiments indicate that there may not be a gap but rather a pseudogap, and the hybridization does not occur over the whole Brillouin zone. Although the temperature dependence of the resistivity in the golden phase of SmS is semiconductor-like, the resistivity is increased only at several times on cooling from a room temperature to $T = 4$ K [22].

Band-structure calculations of golden SmS produce a pseudogap at the Fermi level with a peak just above and a shoulder below the Fermi level were predominantly of f character [23]. When the density of states at E_F is small compared to the giant density of states of the f peaks, the resistivity may nevertheless appear activated over a certain temperature range.

The electrical resistivity of the synthesized $Sm_xMn_{1-x}S$ samples was measured by the four-probe technique in the range of 80–300 K temperatures. The temperature dependences of the resistivity for solid solution are shown in Fig. 2. One can clearly see a gradual change of the temperature dependence of resistivity, which can be divided into two regions: the first extends from 80 to 220 K and the second occupies the range 220–300 K. At first, resistivity decreases and beginning from 220 K the resistivity rises with increasing temperature. It may be explained using a process of electron hopping between Sm^{2+} and Sm^{3+} ions from occupied to empty 5d level by thermal hopping with an activation energy of E_a. The E_a energy value is mainly due to a difference in the energies of local d–f interaction and a deformation of the elastic system near the samarium ion. This causes a fluctuation of potential and the diagonal disorder in terms of Anderson model. The impurity conductivity relies on a disorder diffusion process and drift

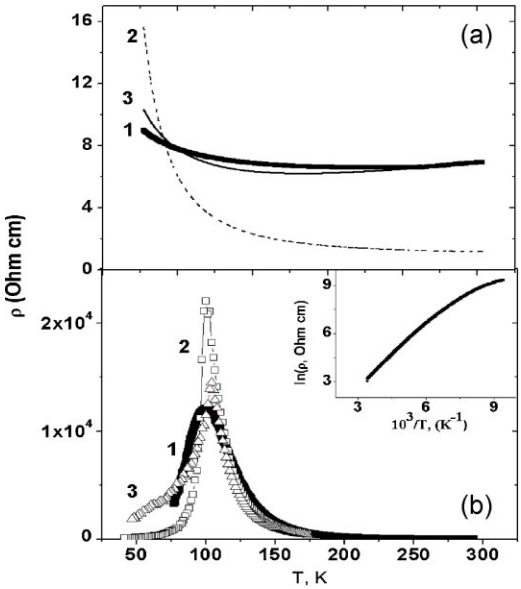

Figure 2 Electrical resistivity versus temperature for (a) $x = 0.15$ compound (curve 1) and the fitting function (1) for parameters $n = 0.1$, $E_a = 410$ eV (2) and $n = 0.01$, $E_a = 186$ eV (3); for (b) $x = 0.2$ compound (curve 1) and calculated in terms of Anderson disordered model using Eq. (2) with $\rho_0 = 0.5\,\Omega$ cm and $W = 3.1$ eV, $\langle S^z\rangle(T)$ (MC) (2), $W = 3$ eV, $\langle S^z\rangle = 0$ (3). The inset shows resistivity versus $10^3/T$ at $T > 100$ K for $Sm_{0.2}Mn_{0.8}S$.

mobility expressed by [24]

$$u = \frac{el^2\omega_p}{k_BT}\exp\frac{-E_a}{k_BT}, \tag{1}$$

where ω_p is the phonon frequency and l is the distance between samarium ions that is approximately equal to $l = x^{1/3}a$. The dependences of resistivity on temperature simulated by the formula $\rho = 1/\sigma = 1/enu$, are presented in Fig. 2a for two fitting parameters: concentration of 5d electrons (n) and E_a activation energy for fixed $\omega_p = 100$ K phonon frequency. An intensity maximum of the phonon mode is observed near the Brillouin-zone boundary, where the frequency of acoustic phonon mode is 66 cm^{-1} in SmS [8] and optical mode 100 cm^{-1} in MnS that proves the validity of the ω_p magnitude used in our simulations. The agreement between theoretical and experimental results is achieved at $n = 0.01$, $E_a = 186$ eV, and $l = 1$ nm. If concentration of current carriers is caused by ions of samarium the relation between divalent and trivalent samarium ions is $Sm^{+3}/Sm^{+2} = 1{:}15$.

The minimum of electrical resistivity may also be explained from by the single-impurity Anderson model that takes into account the crystal-field splitting of the 4f ground-state multiplet, and assumes a strong Coulomb repulsion that restricts the number of f electrons to $n \ll 1$, as a result of the redistribution of the single-particle spectral weight within the Fermi vicinity. If hybridization strength (G) is smaller as compared to crystal-field splitting (D), then the high-temperature maximum in $\rho(T)$ appears. For temperatures below the maximum, $\rho(T)$ drops to a minimum and then rises logarithmically as the coherence temperature T_C is approached. This minimum and the subsequent low-temperature upturn are of a purely electronic origin and appear in systems with small coherence temperature and large crystal-field splitting. The temperatures of maxima and minima in the resistance are related by $T_{min} = T_{max}/3 = D/9k_B$ [25]. Then according to our result $T_{min} = 220$ K have to correspond the magnitude $D = 0.2$ eV of splitting of the 4f ground-state multiplet, that in order of magnitude exceeds splitting of the 4f multiplet in $Sm_xMn_{1-x}S$ solid solution.

The temperature dependence of the electrical resistivity reveals a sharp maximum for $x = 0.2$ (Fig. 2b) that may be caused due to spin density fluctuations in a magnetic ions. According to the modern conception for conductivity in disordered systems, the mobility edge E_C is more important as compared to the activation energy defined between the band edge and the impurity level. We recall that the mobility edge is the energy that separates the localized from the extended states. For magnetic disorder compounds the correlations created by magnetic short-range order are more important for the mobility edge. Using ideas and methods of Anderson localization theory the authors [25] obtain simple formulas that connect the mobility edge with short-range order characteristics of the magnetic subsystem–static spin correlations.

$$\rho = \rho_0\exp\left[\frac{1 - \langle S_0^zS_1^z\rangle/(S^z)^2}{1 + \langle S^z\rangle/S}\left(\frac{W}{4k_BT}\right)\right], \tag{2}$$

where W is the conductivity band width, $\langle S_0^zS_1^z\rangle$ is spin–spin correlator between nearest neighbors, $\langle S^z\rangle$ is average magnetization. We used the Monte Carlo (MC) method for calculation the magnetic characteristics for $18 \times 18 \times 18$, $22 \times 22 \times 22$ size lattice with 50 000–100 000 Monte Carlo steps per site with periodical boundary conditions. Spin–spin correlators $\langle S_0^zS_1^z\rangle$, $\langle S_0^{x,y}S_1^{x,y}\rangle$ are plotted in the insert to Fig. 4 for ferromagnetic (FM) and for antiferromagnetic (AF) with random distribution of FM bonds. Using MC results for $\langle S_0^\alpha S_1^\alpha\rangle$ and $\langle S^z\rangle$ – we fit formula (2) to experimental data with parameter W, ρ. The best agreement is achieved for the band width with $W = 3$ eV, $\rho_0 = 0.5\,\Omega$ cm and spontaneous magnetization tends to zero $\langle S^z\rangle = 0$. A random-bond model with off-diagonal disorder depending on an instant spin configuration gives a quantitative description of the experimental dependence $\rho(T)$. The resistivity peak is a result of the mobility edge movement and the disorder being due to spin–density fluctuations. Increasing of samarium concentration leads to a nonuniform magnetic structure at the same temperature T_c and metal–semiconductors transition versus concentration at $x_c = 0.25$. It is possible that an incommensurable structure is formed at the percolation of Mn–Sm bonds with average magnetization equal to zero. Information about of magnetic properties of $Sm_{0.2}Mn_{0.8}S$ we obtain

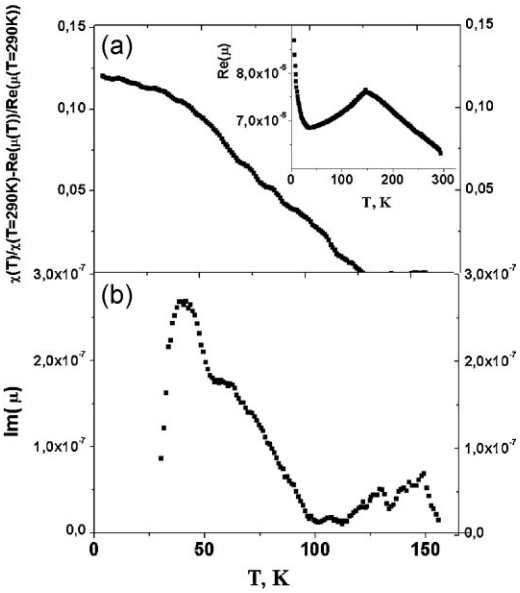

Figure 3 (a) The difference between normalized magnitudes of magnetic susceptibility at the frequency $f = 10$ kHz, $\chi(T)_{nor} = \chi(T)/\chi(T = 290\,K)$, and magnetic permeability $Re(\mu(T))_{nor} = Re(\mu(T))/Re(\mu(T = 290\,K))$ to follow values at $T = 290$ K versus temperature. Inset: Real part of magnetic permeability $Re(\mu)$ at the frequency $f = 10$ kHz versus temperature. (b) Imaginary part of magnetic permeability $Im(\mu)$ for compound $Sm_xMn_{1-x}S$ with $x = 0.2$ at 10 kHz versus temperature.

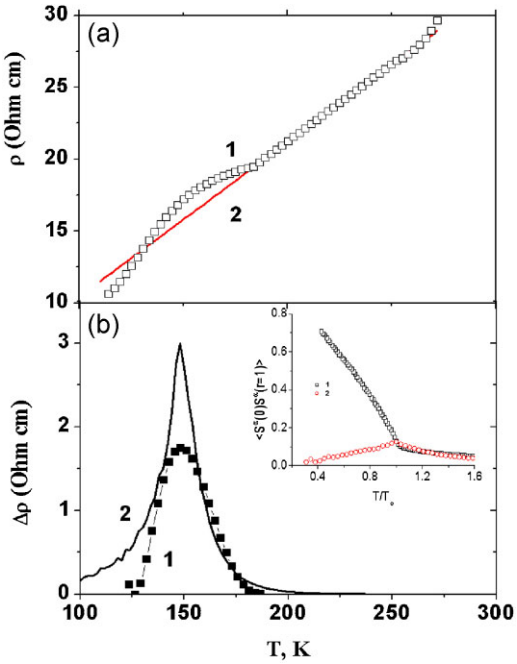

Figure 4 (online color at: www.pss-b.com) (a) Temperature dependence of the electrical resistivity for $x = 0.25$ (1) and the dependence of resistivity versus temperature $\rho(T)/\rho(\Theta) = (T/\Theta)$ (2) as a result of electron–phonon interaction. (b) $\Delta\rho = \rho^{ex} - \rho^{ph}$ (1) and the fitting function (2) with $\rho_0 = 10^{-8}\,\Omega$ cm, $W = 1.2$ eV (2).

from measurement of the real and imaginary part of magnetic permeability at the three frequencies 100 Hz, 1 kHz, and 10 kHz using a Quantum Design PPMS 6000 in the temperature range of $5\,K < T < 300\,K$.

The real part of magnetic permeability $Re(\mu)$ versus temperature is presented in the insert of Fig. 3 for $Sm_xMn_{1-x}S$ samples with $x = 0.2$ at frequency $f = 10$ kHz. A small maximum of $\mu(T)$ may be associated with Neel temperature. The imaginary part of magnetic permeability also has small maximum at $T = T_N$ and starts to rise at $T < 100$ K (Fig. 3). This means a new channel of magnetic moment relaxation appears as a result of the change in magnetic state. Temperature dependencies of $Re(\mu)/Re(\mu(T = 290\,K))$ permeability and $M(T)/M(N = 290\,K)$ magnetization of $Sm_xMn_{1-x}S$ in an external magnetic field differ at $T < 110$ K and the difference between these characteristic is shown in Fig. 3.

At low temperatures the chemical potential lies in the close vicinity of the band edge. At these temperatures the resistivity is defined by the exact position of the chemical potential relative to the band edge; at higher temperatures when E_c moves upward, the dependence of $\rho(T)$ on T is determined mainly by the shift of E_c.

The electrical resistivity for $x = 0.25$ in $Sm_xMn_{1-x}S$ shows a linear dependence with deviation from it near the Neel temperature (Fig. 4a). This is due to electron scattering with acoustic phonon as a result of electron–phonon interaction. Bloch theory predicts a linear dependence of resistivity versus temperature $R(T)/R(\Theta) = (T/\Theta)$ at $T > 2/3\,\Theta$, where Θ – Debye temperature and power dependence is $R(T)/R(\Theta) = (T/\Theta)^5$ at low temperatures $T \ll \Theta$ [26]. Our results $R(T)$ lie well on the linear dependence at $T > 2/3\,\Theta = 180$ K. The Debye temperature can be determined from the relation of resistivity at high and low temperatures $\Theta = T_L[498T_L/T_hR_L/R_h]^{1/4}$. It is impossible to execute for $Sm_xMn_{1-x}S$ compound because a magnetic scattering becomes dominant over phonon scattering at temperature pull down $T < 180$ K. The magnetic contribution to the resistivity is presented in Fig. 4b. The resistivity maximum is explained in terms of scattering electrons on the short range FM order. The fitting of function (2) is plotted in Fig. 4b for parameters $\rho_0 = 10^{-8}\,\Omega$ cm, bandwidth $W = 1.2$ eV and satisfactory agreement with experimental data is seen.

To elucidate the influence of the lattice effect on the formation of a resistivity maximum for $x = 0.2$ compound we carry out measurement of the thermal expansion coefficient a in the temperature range of 100–300 K, that is shown in Fig. 5. Thermal expansion measurements were performed with a heating rate of 3 K/min using a NETZSCH model DIL 402C pushrod dilatometer on samples with $L = 7.88$ mm for $Sm_{0.2}Mn_{0.8}S$ and $L = 1.42$ mm for $Co_{0.05}Mn_{0.95}S$. The results were calibrated by taking SiO_2 as standard reference, removing the influence of system thermal expansion. In the vicinity of $\rho(T)$ the maximum of the coefficient a linearly rises versus temperature, which proves the absence of lattice deformation at $T \sim 100$ K. The Jahn–Teller polaron

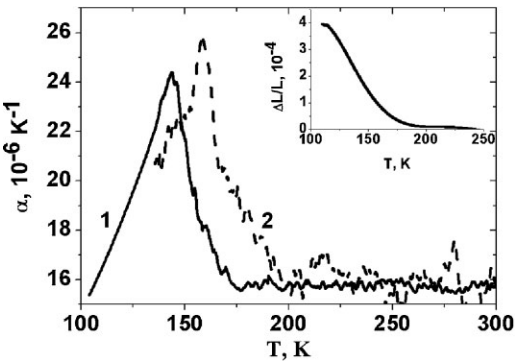

Figure 5 The coefficient of thermal expansion $\alpha(T)$ for $Sm_{0.2}Mn_{0.8}S$ (1) and $Co_{0.05}Mn_{0.95}S$ (2) versus temperature. The inset presents the deformation $\Delta L/L$, due to the magnetic system, versus temperature for $Sm_{0.2}Mn_{0.8}S$.

mechanism suggested by Mills for explanation of resistivity peak in manganese may also be excluding. Below the temperature of antiferromagnetic–paramagnetic phase transition the proportionality between the magnetic part of the a_m and the magnetic heat capacity $C_m(T)$ exists according to the Grüneisen law: $3a_m(T) = GkC_m/\nu$, where G is the magnetic Grüneisen parameter, k the isothermal compressibility, and ν is the specific volume. Parameters G, C_m, and ν are practically temperature independent at $T_N > T > 0.3\ \Theta$ and a have the same temperature dependence as the heat capacity. Taking into account short range magnetic order, C_m can be expressed in the form $C_m = 1/2\ N_z J\ d\langle S_0 S_1\rangle/dT$, where $1/2N_z$ is the number of the nearest-neighbor pairs. For comparison, the thermal expansion coefficient of $Co_xMn_{1-x}S$ is presented in Fig. 5. The substitution of cobalt by manganese retains the antiferromagnetic order [27]. For solid solutions of $Sm_xMn_{1-x}S$ and $Co_xMn_{1-x}S$ the relation $C_{m,Sm}/C_{m,Co}$ is proportional to $\alpha_{Sm}/\alpha_{Co} = 0.92$; and $C_{m,Sm}/C_{m,Co} = [T_{N,Sm}/T_{N,Co}]\ K_{Sm}/K_{Co} = 0.9\ K_{Sm}/K_{Co}$, where $K = d\langle S_0 S_1\rangle/dT$ at $(1 - T/T_N) > 0.1$. As a result, the nearest spin correlator in $Sm_xMn_{1-x}S$, $K_{Sm} = 1.02\ K_{Co}$ weakly dependents on the type of chemical element in $Me_xMn_{1-x}S$ that is justified by the results of spin correlator MC simulations. The temperature-deformation dependence $\Delta L/L$ due to magnetoelastic interaction is shown in the insert to Fig. 5.

3 Conclusion Solid solutions of $Sm_xMn_{1-x}S$ containing samarium ions with mixed valence reveal no evidence for the Kondo effect in the range of temperatures $80 < T < 300$ K. Possibly, the f-state of samarium ions locates below the Fermi level and promotes a small number electrons in the d-subband. The electron state is better described in the disordered Anderson model. The existing f-state near the Fermi level causes a change in conductivity from hopping to band type for $x = 0.15$ as result of interaction of thermoactivation electrons with phonons. The resistivity peak originates from the mobility-edge movement describing in terms of the Anderson model with off-diagonal disorder that arises from formation of nonuniform magnetic order at $T \approx 100$ K. The maximum of the thermal expansion coefficient for $Sm_{0.2}Mn_{0.8}S$ versus temperature is revealed near the Neel temperature attributed to the magnetoelastic interaction. The metal–semiconductors transition versus concentration established for $Sm_{0.25}Mn_{0.75}S$ and the mechanism of electrical resistivity are attributed to scattering electrons on the acoustic phonons and magnetic scattering on uncompensated antiferromagnetic manganese clusters at $T < 180$ K. As a result of substitution of manganese by samarium in the solid solution $Sm_xMn_{1-x}S$ the electronic structure is reconstructed and resistivity could not be explained on the basis of percolation samarium ions since the SmS conductivity behavior differs qualitatively as compared to the $x = 0.25$ compound.

Acknowledgements This study was supported by the Russian Foundation for Basic Research project *No* 09-02-00554_a; No 09-02-92001-NNS_a; No 11-02-98018 r_sibir_a; ADTP "Development of scientific potential of the higher school" No. 2.1.1/11763.

References

[1] O. B. Romanova, L. I. Ryabinkina, V. V. Sokolov, A. Yu. Pichugin, D. A. Velikanov, D. A. Balaev, A. I. Galyas, O. F. Demidenko, G. I. Makovetskii, and K. I. Yanushkevich, Solid State Commun. **150**, 602 (2010).
[2] S. S. Aplesnin, O. N. Bandurina, o. B. Romanova, L. I. Ryabinkina, A. D. Balaev, and E. V. Eremin, J. Phys.: Condens. Matter **22**, 226006 (2010).
[3] W. Ehrenstein, N. Mazur, and J. Scott, Nature **442**, 759 (2006).
[4] A. A. Samochvalov, Magnetic rare-earth semiconductors, in: Rare-Earth Semiconductors (Science, Leningrad, 1997), pp. 5–47.
[5] K. Syassen, Physica B **139–140**, 277 (1986).
[6] V. V. Kaminskii and S. M. Solov'ev, Phys. Solid State **43**, 439 (2001).
[7] V. V. Kaminskii and S. Lanyi, J. Tech. Phys. **43**, 314 (1998).
[8] P. K. Jha, S. P. Sanyal, and R. K. Sing, PINSA **68**, 52 (2002).
[9] T. U. Hailing, G. A. Saunders, and H. Bach, Phys. Rev. B **29**, 1848 (1984).
[10] G. Spronken and M. Avignon, J. Phys. F, Met. Phys. **12**, 2541 (1982).
[11] A. P. Menushenkov, R. V. Chernikov, V. V. Sidorov, K. I. Klementiev, P. A. Alekseev, and A. V. Rybina, JETP Lett. **84**, 119 (2006).
[12] S. S. Aplesnin, G. A. Petrakovskii, L. I. Ryabinkina, G. M. Abramova, N. I. Kiselev, and O. B. Romanova, Solid State Commun. **129**, 195 (2004).
[13] V. V. Kaminskii, N. V. Sharenkova, L. N. Vasil'ev, and S. M. Solov'ev, Phys. Solid State **47**, 225 (2005).
[14] A. B. Andrews, J. J. Joyce, A. J. Arko, Z. Fisk, and P. S. Riseborough, Phys. Rev. B **53**, 3317 (1996).
[15] D. Malterre, M. Grioni, and Y. Baer, Adv. Phys. **45**, 299 (1996).
[16] S. K. Malik, L. Menon, V. K. Pecharsky, and K. A. Gschneidner, Phys. Rev. B **55**, 11471 (1997).
[17] Y. Uwatoko, T. Ishii, G. Oomi, H. Takahasi, N. Moeri, J. D. Thompson, J. L. Shero, D. Madru, and Z. Fisk, J. Phys. Soc. Jpn. **65**, 27 (1996).

[18] N. S. Vidhyadhiraja, A. N. Tahvildar-Zadeh, M. Jarrell, and H. R. Krishnamurthy, J. Europhys. Lett. **49**, 459 (2000).
[19] S. Burdin, A. Georges, and D. R. Grempel, Phys. Rev. Lett. **85**, 1048 (2000).
[20] S. S. Aplesnin, O. B. Romanova, L. I. Ryabinkina, A. M. Har'kov, E. V. Eremin, D. A. Velikanov, V. V. Solokov, A. Yu. Pichugin, O. F. Demidenko, G. I. Makovetskii, and K. I. Yanushkevich, Phys. Status Solidi B **248**, 1975 (2011).
[21] V. N. Antonov, A. P. Shpak, and A. N. Yaresko, J. Condens. Matter Phys. **7**, 211 (2004).
[22] G. Travaglini and P. Wachter, Phys. Rev. B **30**, 5877 (1984).
[23] V. N. Antonov, B. N. Harmon, and A. N. Yaresko, Phys. Rev. B **66**, 165208 (2002).
[24] N. F. Mott, Metal–Insulator Transitions (Taylor & Francis, London, 1974), p. 344.
[25] G. Zlatic and R. Monnier, Phys. Rev. B **71**, 165109 (2005).
[26] E. M. Kogan and M. I. Auslender, Phys. Status Solidi B **147**, 613 (1988).
[27] S. S. Aplesnin, L. I. Ryabinkina, O. B. Romanova, D. A. Velikanov, A. D. Balaev, D. A. Balaev, K. I. Yanushkevich, A. I. Galyas, O. F. Demidenko, and O. N. Bandurina, J. Exp. Theory Phys. **106**, 765 (2008).